Theor Chim Acta (1986) 69: 147–159

Theoretica Chimica Acta

Doubly-charged gas phase cations

G. C. Shields and T. F. Moran

School of Chemistry, Georgia Institute of Technology, Atlanta, GA 30332, USA

(Received September 6/Accepted September 25, 1985)

Unique features of doubly-charged stable organic ions are examined and the results correlated with experimental observations. Self-consistent field molecular orbital methods are used to compute structures and stabilities of $C_nH_2^{2+}$ ($n=2$–9) ions which are prominent in electron impact ionization of hydrocarbon molecules. A simple curve crossing model is employed to rationalize charge transfer reactions of these ions.

Key words: Doubly-charged cations — Stabilities and reactivities

1. Introduction

Atomic doubly-charged ions are produced in high temperature plasmas and both spectroscopic and collisional properties of these atomic ions have been determined [1, 2], but comparatively little is known about long-lived states of doubly-charged molecular ions. These molecular M^{2+} ions are produced by electron impact ionization although their presence is obscured in most cases by singly-charged fragment $(M/2)^+$ ions which possess the same mass-to-charge ratio. Singly- and doubly-charged ions of the same m/e cannot be separated from one another by conventional electrostatic/magnetic analysis. However, the technique of doubly-charged ion mass spectrometry [3] has been developed as an analytical technique to remove singly-charged ions from spectra so that doubly-charged ions can be observed exclusively.

In this method all singly- and doubly-charged ions produced by electron impact in an ion source are fully accelerated into a collision chamber where doubly-charged ions undergo single electron transfer reactions

$$M_r^{2+}(\text{fast}) + N(\text{slow}) \rightarrow M_p^{+}(\text{fast}) + N^{+'}(\text{slow}). \quad (1)$$

Velocities of fast M_p^+ product ions from this reaction are identical to those of the respective keV M_r^{2+} reactant ions. Ions are energy analyzed in an electrostatic sector adjusted to transmit only fast singly-charged M_p^+ product ions into magnetic sector for momentum analysis. These fast product ions appear at a nominal mass M^* given by $(M_p/e)^2/(M_r/2e)$ which unambiguously identifies both reactant and product ions of interaction (1). Ions of the type $C_nH_2^{2+}$ ($n=2$ to 9) have been found to be the most abundant doubly-charged ion species formed in electron impact ionization of hydrocarbon molecules [3-5]. Stable doubly-charged ions have also been observed in charge stripping experiments in which electrons are removed from singly-charged ions during collisions with neutral target molecules [6]. The purpose of the present investigation is to examine the rather unusual structural, energetic and dynamical properties of these $C_nH_2^{2+}$ ions using SCF-MO techniques and to correlate these properties with recent experimental observations.

2. Methods

We have employed the semi-empirical self-consistent field molecular orbital MNDO method developed by Dewar and co-workers [7-10] to describe doubly charged $C_nH_2^{2+}$ ions. This method has been used successfully to obtain geometry optimized minimum energy structures for a large number of hydrocarbon molecules in a reasonably accurate and computationally efficient manner. Calculated heats of formation for several hundred hydrocarbon species are within ~0.3 eV of experimental values. Bond distances and angles are reproduced accurately for both neutral and ionic [7-10] hydrocarbons using this semi-empirical approach.

Minimum energy geometry optimized ionic structures have been determined using the Davidon-Fletcher-Powell method [11]. Energies for various dissociation pathways have been computed for $C_nH_2^{2+}$ ($n=2$-9) ions by computing the geometry optimized, minimum energy of each system at different extensions of a particular bond. Transition state structures, located at the top of barriers for individual dissociation pathways, have also been obtained with the MNDO method. The MNDO potential energy surfaces for ground and transition state structures have been used to compute the respective vibrational frequencies. These frequencies have been calculated from force constants obtained by diagonalizing the Hessian matrix, which is composed of second derivatives of the energy with respect to displacements of all pairs of atoms around their geometry-optimized equilibrium positions. The accuracy of computed frequencies using the semi-empirical SCF method is surprisingly good when compared with experimental data and/or frequencies determined from *ab initio* calculations at the HF/6-31G* level [12, 13].

Spontaneous unimolecular dissociations have been computed for $C_nH_2^{2+}$ ions using the RRKM theory [14]. Frequencies of ground and transition state structures obtained from MNDO computations have been used in the method of Hase and

Bunker [15] to determine $C_nH_2^{2+}$ unimolecular dissociation lifetimes as a function of ion internal energy.

3. Discussion

Potential energy curves computed for these $C_nH_2^{2+}$ ions are rather unique since they possess decomposition barriers several eV higher than asymptotic dissociation energies. General features, characteristic of these potential energy curves, are illustrated in Fig. 1 for $C_2H_2^{2+}$ which is a typical system. The lowest energy decomposition pathway leading to $HC_2^+ + H^+$ products follows a Coulomb repulsive potential curve at large separation distances. The $C_2H_2^{2+}$ ion energy (eV), relative to ground state C_2H_2 molecules, is displayed as a function of $[HC_2\cdots H]^{2+}$ separation distance (Å). Dissociation products are indicated by the horizontal line at infinite separation distance. The insert illustrates the potential energy curve over a more limited range of separation distance near the barrier maximum. The barrier maximum is 3.4 eV above the potential well minimum.

Bond lengths for geometry optimized minimum energy structures of the type $C_nH_2^{2+}$ and their respective transition states leading to singly-charged decomposition products are given in Table 1. All ground state ions and transition state structures are linear. Ground states of $C_2H_2^{2+}$, $C_4H_2^{2+}$ and $C_6H_2^{2+}$ ions are triplets, while ground states of all other ions are singlets. Dissociative $[HC_n\cdots H]^{2+}$ transition states possess larger terminal C_{n-1}—C_n bond lengths than corresponding bond lengths of ground state ion structures. The remaining C—C bond length changes display an alternating increase-decrease pattern when comparing transition state with ground state geometries. Energy differences between ground state $C_nH_2^{2+}$ ($n = 2$ to 9) ions and their dissociative $[HC_n\cdots H]^{2+}$ and $[HC_m\cdots C_{n-m}H]^{2+}$ transition states are presented in Table 2. Energy differences are relatively large and range from 3.44 to 8.24 eV. These potential wells have sufficiently high barriers

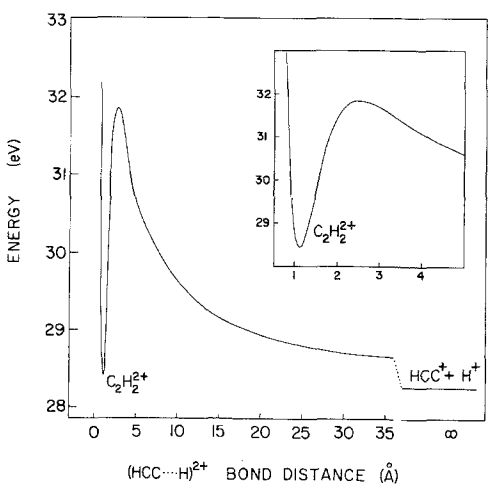

Fig. 1. Potential energy curve for dissociation of $C_2H_2^{2+}$ into HCC^+ and H^+ products. The insert illustrates potential energy variation for separation distances less than 5 Å

Table 1. Bond lengths (Å) for $C_nH_2^{2+}$ ions and dissociative $[HC_n\cdots H]^{2+}$, $[HC_m\cdots C_{n-m}H]^{2+}$ transition states[a]

Ion	$R(C_1H_1)$	$R(C_1C_2)$	$R(C_2C_3)$	$R(C_3C_4)$	$R(C_4C_5)$	$R(C_5C_6)$	$R(C_6C_7)$	$R(C_7C_8)$	$R(C_8C_9)$	$R(C_n\cdots H)$
$C_2H_2^{2+}(T)$	1.096	1.367								1.096
$[HC_2\cdots H]^{2+}$	1.079	1.380								2.447
$C_3H_2^{2+}(S)$	1.086	1.277	1.277							1.086
$[HC_3\cdots H]^{2+}$	1.074	1.246	1.322							2.602
$C_4H_2^{2+}(T)$	1.078	1.296	1.289	1.296						1.078
$[HC_4\cdots H]^{2+}$	1.067	1.283	1.285	1.330						2.775
$C_5H_2^{2+}(S)$	1.075	1.248	1.301	1.301	1.248					1.074
$[HC_5\cdots H]^{2+}$	1.066	1.226	1.327	1.262	1.302					2.891
$C_6H_2^{2+}(T)$	1.070	1.268	1.293	1.295	1.293	1.268				1.070
$[HC_6\cdots H]^{2+}$	1.062	1.254	1.299	1.294	1.276	1.312				2.990
$[HC_3\cdots C_3H]^{2+}$	1.067	1.272	1.266	2.655	1.337	1.238				1.071
$C_7H_2^{2+}(S)$	1.068	1.234	1.316	1.272	1.272	1.316	1.234			1.068
$[HC_7\cdots H]^{2+}$	1.061	1.216	1.339	1.239	1.309	1.268	1.296			3.181
$[HC_4\cdots C_3H]^{2+}$	1.070	1.236	1.340	2.658	1.223	1.324	1.266			1.064
$[HC_5\cdots C_2H]^{2+}$	1.064	1.223	1.331	1.256	1.312	2.923	1.270			1.074
$C_8H_2^{2+}(S)$	1.066	1.254	1.300	1.300	1.281	1.300	1.300	1.254		1.066
$[HC_8\cdots H]^{2+}$	1.060	1.231	1.318	1.277	1.283	1.298	1.280	1.312		3.499
$[HC_5\cdots C_3H]^{2+}$	1.063	1.219	1.336	1.248	1.326	3.464	1.352	1.231		1.068
$C_9H_2^{2+}(S)$	1.064	1.228	1.324	1.260	1.289	1.289	1.260	1.324	1.228	1.064
$[HC_9\cdots H]^{2+}$	1.058	1.212	1.346	1.231	1.322	1.248	1.302	1.270	1.295	3.574
$[HC_5\cdots C_4H]^{2+}$	1.063	1.220	1.334	1.252	1.318	2.800	1.226	1.321	1.265	1.063
$[HC_6\cdots C_3H]^{2+}$	1.061	1.235	1.311	1.288	1.272	1.328	3.648	1.355	1.230	1.067

[a] Each of these ground state ions and their transition states are linear. The symbols T (triplet) and S (singlet) indicate the multiplicity of the ground state $C_nH_2^{2+}$ ion

Table 2. Energy differences (eV) between ground state $C_nH_2^{2+}$ ions and their dissociative $[HC_n\cdots H]^{2+}$, $[HC_m\cdots C_{n-m}H]^{2+}$ transition states, excess energies (eV) above the transition state needed for dissociation in 8-15 μseconds and the total energies (eV) above the ground state needed for dissociation

Ion	Transition state	E (Transition state) $-E$ (Ground state ion)	Excess energy for dissociation in 8-15 μseconds	Total energy required for dissociation in 8-15 μseconds
$C_2H_2^{2+}(T)$	$[HC_2\cdots H]^{2+}$	3.437	—	—
$C_3H_2^{2+}(S)$	$[HC_3\cdots H]^{2+}$	4.208	0-0.004	4.21-4.212
$C_4H_2^{2+}(T)$	$[HC_4\cdots H]^{2+}$	4.894	0.26-0.28	5.15-5.17
$C_5H_2^{2+}(S)$	$[HC_5\cdots H]^{2+}$	5.380	0.61-0.66	5.99-6.04
$C_6H_2^{2+}(T)$	$[HC_6\cdots H]^{2+}$	5.846	1.08-1.17	6.93-7.02
	$[HC_3\cdots C_3H]^{2+}$	6.484	1.30-1.41	7.78-7.89
$C_7H_2^{2+}(S)$	$[HC_7\cdots H]^{2+}$	6.181	1.73-1.82	7.91-8.00
	$[HC_4\cdots C_3H]^{2+}$	7.638	1.82-1.99	9.46-9.63
	$[HC_5\cdots C_2H]^{2+}$	8.238	1.78-1.91	10.02-10.15
$C_8H_2^{2+}(S)$	$[HC_8\cdots H]^{2+}$	6.632	2.60-2.73	9.23-9.36
	$[HC_5\cdots C_3H]^{2+}$	5.079	1.71-1.82	6.79-6.90
$C_9H_2^{2+}(S)$	$[HC_9\cdots H]^{2+}$	6.764	2.93-3.10	9.69-9.86
	$[HC_5\cdots C_4H]^{2+}$	7.712	3.42-3.56	11.13-11.27
	$[HC_6\cdots C_3H]^{2+}$	6.615	2.12-2.25	8.74-8.86

to enable $C_nH_2^{2+}$ ions to survive even though they may possess internal excitation energy in excess of asymptotic dissociation limits. Thus, it is not surprising that these stable $C_nH_2^{2+}$ ions, formed by 100 eV electron impact ionization-fragmentation of hydrocarbon molecules, are abundant in the doubly-charged ion mass spectra of organic molecules.

Although stable ions of the type $C_nH_2^{2+}$ have been found to be ubiquitous in doubly-charged ion mass spectra, a recent investigation [16] has shown that a small fraction of the total number of $C_nH_2^{2+}$ ions undergo spontaneous unimolecular dissociation 8-15 μs after formation. This latter observation indicates $C_nH_2^{2+}$ ions are formed with internal energy distributions extending above the respective barriers to dissociation. In order to examine the dependence of spontaneous dissociation processes of these ions with excess internal energy we have employed the RRKM approach with input frequencies from MNDO computations of ground state and saddle point structures.

Vibrational frequencies have been determined from force constants obtained by diagonalizing the Hessian matrix composed of second derivatives of energy with respect to displacements of all pairs of atoms around their geometry-optimized equilibrium positions. It has been shown [17-19] that *ab initio* calculations of molecular vibrational frequencies at the *HF*/6-31G* level of theory result in frequencies that are slightly larger than experimental values. Scaling procedures [17-19] have been used to bring theoretical frequencies into line with experiment.

A uniform scale factor of 0.89 was chosen [19] from the ratio {$\Delta G(0_i)$experiment}/{ν_i from *HF*/6-31G* theory}, where $\Delta G(0_i)$ is the measured $0 \rightarrow 1$ energy difference of the ith vibrational mode of frequency ν_i. This value of the scaling factor was determined from comparisons of 165 frequencies of first-row molecules and has been used with success to predict vibrational frequencies of other molecules and ions [19]. Similar comparison of $\Delta G(0_i)$ experimental values with MNDO computed frequencies has led us [13] to adopt a uniform scaling factor of 0.91. Scaled vibrational frequencies calculated for both ground state $C_nH_2^{2+}$ ions and transition state structures associated with lower energy decomposition channels are presented in Table 3. Degenerate frequencies are denoted by a superscript a. Each transition state possesses one vibrational frequency less than the corresponding ground state since the force constant matrix for the transition state contains one negative eigenvalue associated with motion along the reaction coordinate. It is noticed that the magnitudes of several transition state bending modes are reduced while stretching modes are generally increased in transition state structures. Similar frequency shifts between ground state and saddle point transition state structures have been noted by Hase and Wolf [20] in their analysis of C_2H dissociation.

Unimolecular RRKM dissociation lifetimes for $[HC_n \cdots H]^{2+}$ deprotonation channels of individual ions are presented graphically in Fig. 2 as a function of excess energy (eV) above individual dissociation maxima. As the molecular weight is increased, successively more internal energy is required to achieve dissociation

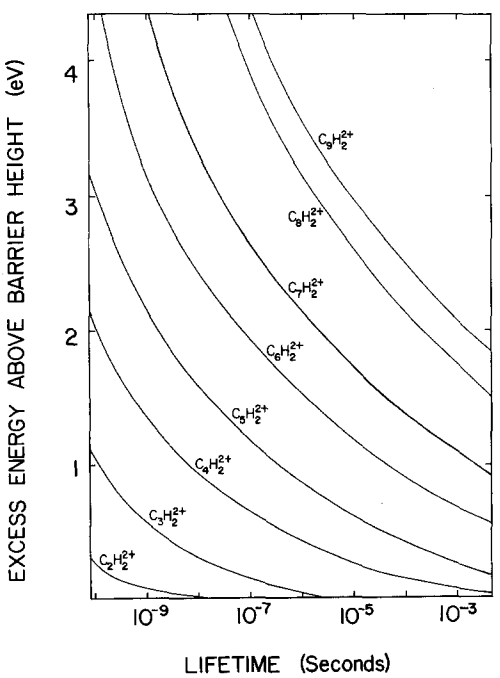

Fig. 2. Lifetimes for dissociation of $C_nH_2^{2+}$ ions into HC_n^+ and H^+ products, as a function of excess internal energy above the potential energy barrier maxima

Table 3. Calculated vibrational frequencies of ground state $C_nH_2^{2+}$ ions and dissociative $[HC_n\cdots H]^{2+}$, $[HC_m\cdots C_{n-m}H]^{2+}$ transition states

Ion	Frequencies (cm^{-1})
$C_2H_2^{2+}(T)$	2891, 2831, 1511, 721[a], 678[a]
$[HC_2\cdots H]^{2+}$	2032, 1496, 576[a], 268[a]
$C_3H_2^{2+}(S)$	2997, 2988, 1982, 1273, 916[a], 896[a], 460[a]
$[HC_3\cdots H]^{2+}$	3122, 2014, 1272, 906[a], 488[a], 222[a]
$C_4H_2^{2+}(T)$	3055, 3042, 2098, 1482, 953, 777[a], 773[a], 561[a], 262[a]
$[HC_4\cdots H]^{2+}$	3153, 2032, 1474, 955, 734[a], 545[a], 294[a], 168[a]
$C_5H_2^{2+}(S)$	3112, 3111, 2087, 1989, 1539, 889[a], 887[a], 792, 704[a], 434, 415, 230, 180
$[HC_5\cdots H]^{2+}$	3204, 2112, 2004, 1513, 877[a], 798, 698[a], 439[a], 224[a], 141[a]
$C_6H_2^{2+}(T)$	3137, 3129, 2137, 1791, 1643, 1240, 798, 797[a], 790, 661, 634, 626, 516, 491, 306, 296, 260, 125
$[HC_6\cdots H]^{2+}$	3213, 2081, 1760, 1633, 1233, 765[a], 665, 616[a], 501[a], 315[a], 185[a], 110[a]
$[HC_3\cdots C_3H]^{2+}$	3163, 3156, 2014, 1566, 1259, 1246, 907, 904, 885, 621, 468, 460, 427, 401, 273, 105, 93, 51
$C_7H_2^{2+}(S)$	3174, 3173, 2114, 2085, 1953, 1658, 1112, 880[a], 879[a], 721[a], 624[a], 580, 419[a], 242, 238, 108, 95
$[HC_7\cdots H]^{2+}$	3248, 2145, 2100, 1970, 1608, 1117, 866[a], 708[a], 616[a], 584, 417[a], 254[a], 146[a], 83[a]
$[HC_4\cdots C_3H]^{2+}$	3193, 3163, 2016, 1874, 1650, 1249, 945, 903[a], 752, 734, 478, 467, 462[a], 241[a], 93, 86, 44, 40
$[HC_5\cdots C_2H]^{2+}$	3216, 3086, 2116, 2006, 1627, 1497, 875[a], 795, 694, 634, 433[a], 372, 328, 196[a], 166, 68, 54, 19
$C_8H_2^{2+}(S)$	3178, 3177, 1768, 1767, 1623, 1536, 1382, 952, 890[a], 746[a], 626[a], 544[a], 486, 460[a], 317[a], 177[a], 71[a]
$[HC_8\cdots H]^{2+}$	3243, 1856, 1770, 1667, 1594, 1350, 947, 875, 785, 643, 578, 572, 536, 488, 469, 442, 320, 305, 188, 182, 121, 117, 94, 62
$[HC_5\cdots C_3H]^{2+}$	3234, 3187, 2135, 2024, 2008, 1475, 1235, 900[a], 871[a], 796, 688[a], 447[a], 422, 417, 180, 165, 111, 44, 33[a]
$C_9H_2^{2+}(S)$	3209, 3205, 2077, 1961, 1956, 1762, 1698, 1279, 884, 863[a], 863[a], 707[a], 655[a], 571[a], 450, 408[a], 277[a], 151[a], 58
$[HC_9\cdots H]^{2+}$	3273, 2117, 2059, 1962, 1640, 1542, 1274, 890, 851[a], 697[a], 646[a], 563[a], 449, 404[a], 279[a], 162[a], 95[a], 49[a]
$[HC_5\cdots C_4H]^{2+}$	3226, 3203, 2123, 2010, 1868, 1630, 1487, 953, 873[a], 793, 747, 729, 691[a], 476, 463, 429[a], 237[a], 191[a], 65, 60, 57, 27
$[HC_6\cdots C_3H]^{2+}$	3237, 3192, 2041, 2017, 1802, 1680, 1238, 1229, 900[a], 822[a], 669, 609[a], 495[a], 444[a], 292[a], 125[a], 34, 28[a], 14

[a] Indicates degenerate frequencies

within a specific lifetime range. Data displayed in Fig. 2 illustrate that dissociation of excited $C_2H_2^{2+}$ ions will be complete in less than 10^{-7} s and these ions will not be metastable on the μs time scale: a fact in accord with the measurements of Ref. [16]. Dissociative lifetimes for reaction channels involving C—C scissure processes are given in Fig. 3 for $C_nH_2^{2+}$ ($n = 6$–9) ions that have been observed to dissociate in 8–15 μs. Although the excess internal energies above the dissociation barriers required for $C_{8,9}H_2^{2+}$ deprotonations are large, the excess energy

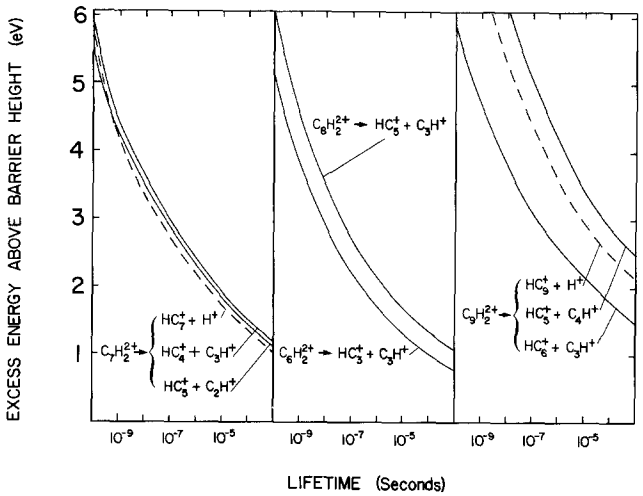

Fig. 3. Lifetimes for dissociations of $C_nH_2^{2+}$ ions ($n = 6$–9) as a function of excess internal energy above potential energy barrier maxima

requirements are relatively low for unimolecular dissociation processes giving rise to C_5H^+ and C_6H^+ product ions from $C_8H_2^{2+}$ and $C_9H_2^{2+}$ respectively. These latter products are the most abundant ions found [16] in the unimolecular (8–15 μs) dissociation spectra of $C_nH_2^{2+}$ ($n = 8$–9) ions. In general, the data in Fig. 3 show that unimolecular decomposition in 8 to 15 μs requires $C_nH_2^{2+}$ (6–9) ions to be formed with excess energy several eV above the barrier maxima given in Table 2.

Single electron transfer reactions of $C_nH_2^{2+}$ ions occur readily with a wide variety of target molecules and the analytical application of doubly-charged ion mass spectrometry takes advantage of this property. In order to gain insight into these reactions we have employed a diabatic curve crossing model [21] which has been used previously to describe single electron transfer reactions of doubly-charged atomic ions [22]. We have chosen the reaction

$$C_2H_2^{2+}(\text{fast}) + C_2H_2(\text{slow}) \rightarrow C_2H_2^+(\text{fast}) + C_2H_2^+(\text{slow}) + \Delta E \qquad (2)$$

involving acetylene as a model system for detailed study. Energetics for charge transfer reactions in the acetylene system are illustrated in Fig. 4 where the $C_2H_2^{2+} \rightarrow C_2H_2^+/C_2H_2 \rightarrow C_2H_2^+$ "half-reactions" are presented. Electron transfer processes involving keV ions occur in time periods short compared to nuclear motion and as a first approximation the Franck-Condon principle applies [23]. Descending vertical lines denote ionic recombination energies; the energies liberated when a single electron combines with $C_2H_2^{2+}$ to form $C_2H_2^+$ products. Recombination energies have been obtained from SCF-MO computations by determining the energy difference between $C_2H_2^{2+}$ and $C_2H_2^+$ ions, "frozen" in the configuration of the geometry optimized minimum energy $C_2H_2^{2+}$ reactant ion. The solid curve at the right side of Fig. 4 illustrates the Franck-Condon ionization envelope obtained from the photoelectron spectrum [24] of C_2H_2 target

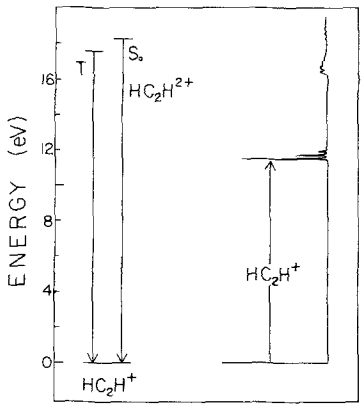

Fig. 4. Energetics of single electron transfer processes involving HC_2H^{2+} ions. Energies liberated in the $HC_2H^{2+} \rightarrow HC_2H^+$ process are given by *descending vertical lines.* The Franck-Condon envelope for ionization of acetylene target gas is represented by the photoelectron spectrum taken from the work of Kimura et al [24]

molecules. The long range interaction energy of $C_2H_2^{2+}$ doubly-charged ions approaching neutral target molecules is approximated by ion-dipole and ion-induced dipole terms of the form

$$V = \frac{-Ze\mu}{R^2}\cos\theta - \frac{Z^2e^2\alpha(C_2H_2)}{2R^4}, \tag{3}$$

where e is the electronic charge, μ is the dipole moment of the target molecule, R is the ion-molecule separation distance, θ is the orientation angle of the dipole with respect to R, and α is the polarizability of the C_2H_2 target molecule. The dipole moment of C_2H_2 is zero, so that the first term in Eq. (3) vanishes in this particular reaction. The leading terms in the interaction potential which describes singly-charged $C_2H_2^+$ product species are Coulombic repulsive and ion-induced dipole attractive potentials of the form suggested by Kamber et al. [22]

$$V = \frac{e^2}{R} - \frac{e^2}{2R^4}[\alpha(C_2H_2^+) + \alpha(C_2H_2^+)] - \Delta E, \tag{4}$$

where α is the polarizability of $C_2H_2^+$ product ions computed by the methods of [25, 26] and ΔE is the energy defect of reaction (2). These approximate potential energy curves for incoming reactants and outgoing products of single electron transfer are displayed in Fig. 5. Product ion interactions are shown for the calculated Franck-Condon neutralization of $C_2H_2^{2+}$ reactant ions to form ground state $C_2H_2^+(\Pi_u)$ ions, whereas C_2H_2 target molecules may ionize to form either Π_u, Σ_g, or Σ_u product ion states. Possible $(C_2H_2^+ + C_2H_2^+)$ product channel curves are labelled $\Pi_u - \Pi_u$, $\Pi_u - \Sigma_g$, and $\Pi_u - \Sigma_u$. Each curve terminates at the respective $C_2H_2^+$ ionic state represented on the right side of the figure by the photoelectron spectrum of [24]. As indicated in this figure, diabatic transitions between the reactant channel and the exothermic $C_2H_2^+(^2\Pi_u) + C_2H_2^+(^2\Pi_u)$ product channel are possible at an ion-molecule separation distance of approximately 2.5 Å. This 2.5 Å ion-molecule separation is consistent with the "reaction window" proposed by Smith et al. [27] to exist between 2 and 6 Å where large rate coefficients were

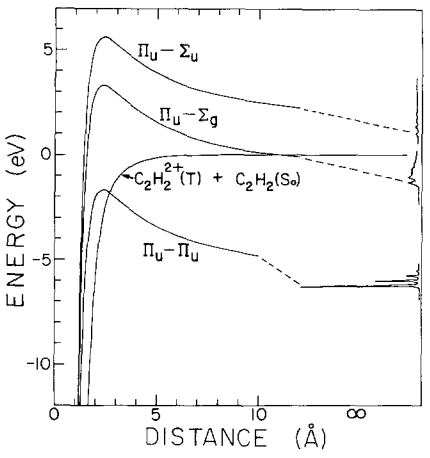

Fig. 5. Potential energy curves for $HCCH^{2+}(T)+HCCH(S_0)$ interactions as a function of ion-molecule separation distance. Single electron transfer product channels which lead to various states of $HCCH^+ - HCCH^+$ product systems are designated by the curves labeled $\Pi_u - \Sigma_u$, $\Pi_u - \Sigma_g$ and $\Pi_u - \Pi_u$

observed for electron transfer reactions of doubly-charged atomic ions with neutral targets.

Curve crossings at similar separation distances are expected in general for $\{C_nH_2^{2+} + (\text{molecule})\}$ interactions involving different reactant ion-molecule systems. Polarizabilities and reaction energy defects largely control curve crossings. Recombination energies for $C_nH_2^{2+} \rightarrow C_nH_2^+$ Franck-Condon "half reactions" displayed in Table 4 decrease in magnitude from 17.6 eV to 11.6 eV as n increases from 2 to 9. Product curves are shifted to more positive values of ΔE as recombination energies are decreased, resulting in reactant/product curve crossings at larger distances. However, this trend is compensated partially by product $C_nH_2^+$ ion polarizability values shown in Table 4 which increase by an order of magnitude as n changes from 2 to 9. Larger ion polarizabilities tend to lower product curves and shift crossing points to smaller distances. It is to be noted that recombination energies associated with $C_nH_2^{2+}$ ions are larger than typical

Table 4. Electron-ion recombination energies (RE) of $C_nH_2^{2+}$ ions and product $C_nH_2^+$ ion polarizablities[a]

n	$C_nH_2^{2+}$ $R.E.$ (eV)	$C_nH_2^+$ polarizabilities $\bar{\alpha}$ (10^{-24} cm^3)
2	17.62	3.205
3	15.12	4.745
4	15.21	7.543
5	13.48	10.103
6	13.77	14.324
7	12.41	17.834
8	12.50	24.445
9	11.65	27.975

[a] Determined for ions formed in vertical Franck-Condon $C_nH_2^{2+} \rightarrow C_nH_2^+$ transitions

hydrocarbon ionization potentials and single electron transfer reactions involving a wide range of target molecules are all exothermic.

Although curve crossings to produce $C_2H_2^+(\Pi_u)$ products in Fig. 4 fall within the proposed "reaction window", this 2.5 Å separation distance is sufficiently small to question the general use of long range potentials (Eqs. 3, 4) to describe these ion-molecule reactions. In order to examine these interactions in greater detail, we have employed the SCF-MO treatment to determine the energies of $C_4H_4^{2+}$ pseudo-molecular complexes formed from collisions of $C_2H_2^{2+}$ with C_2H_2 target molecules at specified orientations. The results of these computations are presented in Fig. 6 where the interaction energies of $(C_2H_2^{2+}+C_2H_2)$ reactant complexes are given as a function of ion-molecule separation distance for the three geometric approaches considered below:

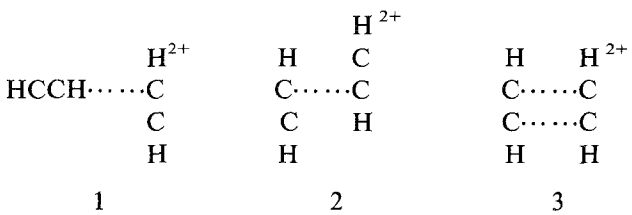

Interaction potential curves were obtained by incrementing the ion-molecule separation distance and calculating the energy for the system. The lowest energy configuration was computed for geometry 3, and as shown in Fig. 6 this interaction potential intersects the product channel curve at a centre-of-mass separation distance of 2.8 Å. The potential curve for the perpendicular collision system 1 does not cross the $C_2H_2^+(\Pi_u)+C_2H_2^+(\Pi_u)$ product curve and is not expected to yield $C_2H_2^+(\Pi_u)$ products efficiently in single electron transfer reactions. In an extension of the SCF-MO computational model, the colliding ion-molecule pair

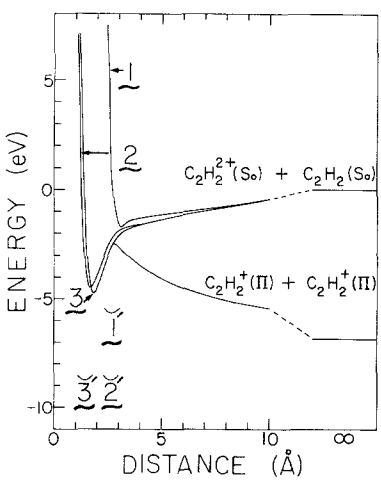

Fig. 6. Interaction potential energies for three orientations of the $HCCH^{2+}+HCCH$ colliding pair. Curves for the three different ion-molecule configurations (1, 2 and 3) are given as solid curves extrapolated to $HCCH^{2+}+HCCH$ at large distances. The single electron transfer product curve is labeled by the $HCCH^+(\Pi)+HCCH^+(\Pi)$ designation

was allowed to relax to the minimum energy $C_4H_4^{2+}$ ion complex formed from the initial reactant configuration. The three geometry optimized structures are indicated below and are denoted by primes:

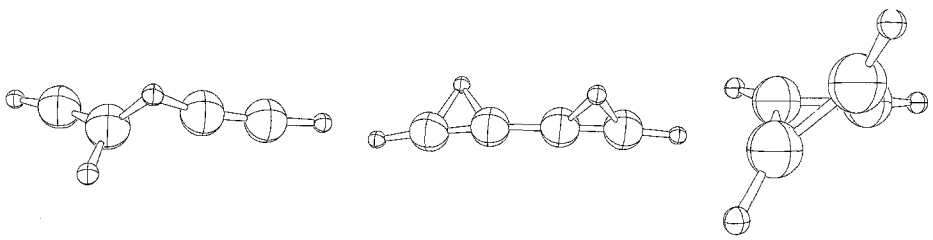

1′ 2′ 3′

Energies of these geometry optimized structures are denoted in Fig. 6 by 1′, 2′, and 3′. The offset parallel (2) and parallel (3) ion-molecule approaches produce geometry optimized systems (2′ and 3′) of similar energies but vastly different structures. While the 2′ structure has a nearly linear carbon chain, the 3′ ion-molecule system minimizes to a twisted cyclic structure expected for the cyclobutadiene dictation. Such rearrangements are not expected for interaction times appropriate to keV $C_nH_2^{2+}$ ion reactions with the result that long range forces (Eqs. 2, 3) generally control curve crossing points.

4. Conclusion

Structures, stabilities and reactivities of $C_nH_2^{2+}$ ions have been examined. These ionic species are linear and exist in deep potential wells with high dissociation barriers. Single electron transfer reactions involving these doubly-charged ions occur with a wide variety of target molecules and these reactions have been interpreted by invoking diabatic transitions between reactant and product potential energy curves at moderately large separation distances.

References

1. Marrus R (ed) (1983) Atomic physics of highly ionized atoms. Nato Advanced Science Series B, Physics 96. Plenum Press, New York.
2. Dijkkamp D, Ćirić D, deHeer F J (1985) Phys Rev Lett 54:1004.
3. Jones BE, Abbey LE, Chatham HL, Hanner AW, Teleshefsky LA, Burgess EM, Moran TF (1982) Org Mass Spectrom 17:10
4. Appling JR, Jones BE, Abbey LE, Bostwick DE, Moran TF (1983) Org Mass Spectrom 18:282
5. Appling JR, Musier KM, Moran TF (1984) Org Mass Spectrom 19:412
6. Rabrenović M, Proctor C J, Ast T, Herbert C G, Brenton A G, Beynon JH (1983) J Phys Chem 87:3305
7. Bingham RC, Dewar MJS, Lo DH (1975) J Am Chem Soc 97:1285; 97:1294; 97:1302; 97: 1307
8. Dewar MJS, Lo DH, Ramsden CA (1975) J Am Chem Soc 97:1311
9. Dewar MJS, Rzepa HS (1977) J Am Chem Soc 99:7432
10. Dewar MJS, Thiel W (1977) J Am Chem Soc 99:4899; 99:4907

11. Davidon WC (1968) Comput J 10:406; Fletcher R (1965) Comput J 8:33; Fletcher R, Powell MJD (1963) Comput J 6:163
12. Dewar MJS, Ford GP (1977) J Am Chem Soc 99:1685
13. Appling JR, Moran TF (1985) Chem Phys Lett 118:188
14. Robinson PJ, Holbrook KA (1972) Unimolecular reactions. Wiley-Interscience, New York
15. Hase WL, Bunker DL (1973) QCPE 11:234
16. Rabrenović M, Beynon JH (1983) Int J Mass Spectrom Ion Processes 54:87
17. Fogarasi G, Pulay P (1984) Ann Rev Phys Chem 35:191
18. Raine GP, Schaefer III HF (1984) J Chem Phys 81:4034
19. De Frees DJ, McLean AD (1985) J Chem Phys 82:333
20. Hase WL, Wolf RJ (1981) J Chem Phys. 75:3809
21. Johnson RE, Boring JW (1978) In: Cooks RG (ed) Collision spectroscopy. Plenum Press, New York
22. Kamber EY, Brenton AG, Beynon JH, Hasted JB (1985) J Phys B: At Mol Phys 18:933
23. Moran TF (1984) In: Christophorou LG (ed) Electron molecule interactions and their applications. Academic Press, New York
24. Kimura K, Katsumata S, Achiba Y, Yamazaki T, Iwata S (1981) Handbook of HeI photoelectron spectra of fundamental organic molecules. Japan Scientific Societies Press, Tokyo
25. Dewar MJS, Yamaguchi Y, Suck SH (1978) Chem Phys Lett 59:541
26. Stewart JJP (1983) QCPE 13:455
27. Smith D, Adams NG, Alge E, Villinger H, Lindinger W (1980) J Phys B: At Mol Phys 13:2787